6th European Conference on Computational Mechanics (ECCM 6)
7th European Conference on Computational Fluid Dynamics (ECFD 7)
11–15 June 2018, Glasgow, UK

EXACT FLAME-FRONT TRACKING IN PREMIXED LOW MACH NUMBER COMBUSTION

Clemens Gößnitzer and Herbert Steinrück

Institute of Fluid Mechanics and Heat Transfer, TU Wien,
Getreidemarkt 9, A-1060 Vienna, Austria. http://www.fluid.tuwien.ac.at
{clemens.goessnitzer,herbert.steinrueck}@tuwien.ac.at

Key words: Premixed Combustion, Flame-Flow Interaction, Flame Front Tracking, Low Mach Number Approximation, Boundary Element Method

Abstract. Slow combustion is considered under the assumption of an infinitely thin flame front. We present a tracking method which fulfills the jump conditions at the flame front by using marker points and a singular volumetric flux source at the interface. Due to the low Mach number assumption, Helmholtz decomposition of the velocity field is used to solve two easier sub-problems. Comparison of the flame shape with level set CFD solutions yields good agreement.

1 INTRODUCTION

Numerical investigation of combustion and flame propagation is a complex problem on multiple scales. One has to account for chemical reactions, gas dynamics and interface tracking in a highly non-steady problem. However, many industries require a reliable and good prediction of the behaviour of flammable fluids. As an example, the design of dust explosion suppression devices requires knowledge of the development of the flame front and pressure–time evolution.

Two major levels of modelling detail can be distinguished: (I) accounting for chemical reactions, kinetics and different species combined with computational fluid dynamics, and (II) models which reduce the flame to an infinitely thin interface. The second approach, called flame sheet model, is used here.

Darrieus[1] and Landau[2] were one of the first to use a gasdynamic model for flame propagation, treating the flame front as a discontinuity. However, their model is unconditionally unstable which contradicts observation. Thus, Markstein[3] added a postulated stabilisation mechanism to better agree with experiments. More complex models for the flame front description were developed by Shivashinsky[4], Matalon and Matkowsky[5] and Class et al.[6]. Here, we use the Markstein model because of its simplicity.

All simulations which use the flame sheet model require a method to keep track of the flame front. Current state of the art are level-set or volume of fluid methods. Both use a scalar quantity which is transported with the flame front to describe the position of the interface. Both require solving at least one additional partial differential equation.

Furthermore, the exact position of the flame front is unknown. Our approach is to track the flame front with marker points which move with the front. The goal is to simplify the flame front tracking to allow for fast predictions of flame propagation.

2 PHYSICAL MODEL

We consider premixed combustion of an ideal gas. Our focus is on closed geometries of arbitrary shape. However, the method described here is equally valid for any slow combustion. Therefore, we will keep the description as general as possible.

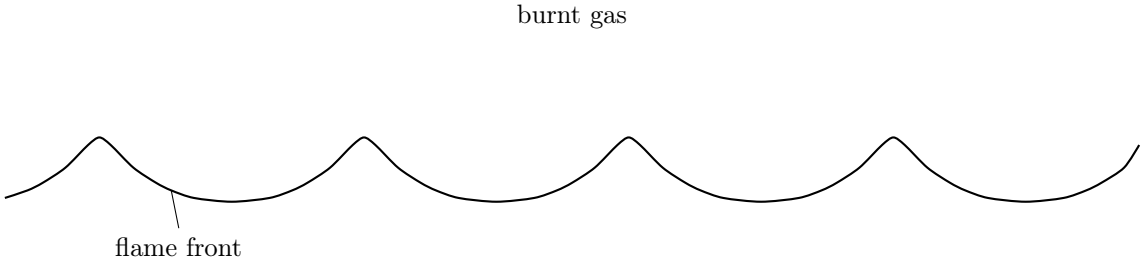

Figure 1: A flame front moves into unburnt gas

2.1 Governing Equations

A flame front separates unburnt, fresh gas from already burnt gas (Figure 1). In both phases, conservation of mass, momentum and energy have to be fulfilled. We neglect friction and heat conduction. The tilde indicates that a quantity has a dimension:

$$\frac{\partial \tilde{\varrho}}{\partial \tilde{t}} + \tilde{\nabla} \cdot (\tilde{\varrho}\tilde{\boldsymbol{u}}) = \tilde{0}, \tag{1}$$

$$\frac{\partial (\tilde{\varrho}\tilde{\boldsymbol{u}})}{\partial \tilde{t}} + \tilde{\nabla} \cdot (\tilde{\varrho}\tilde{\boldsymbol{u}}\tilde{\boldsymbol{u}}) = -\tilde{\nabla}\tilde{p}, \tag{2}$$

$$\frac{\partial \left(\tilde{\varrho}\left(\tilde{e} + \tilde{u}^2/2\right)\right)}{\partial \tilde{t}} + \tilde{\nabla} \cdot \left(\tilde{\varrho}\left(\tilde{e} + \tilde{u}^2/2\right)\tilde{\boldsymbol{u}}\right) = -\tilde{\nabla} \cdot (\tilde{p}\tilde{\boldsymbol{u}}), \tag{3}$$

with time $\tilde{t}$, density $\tilde{\varrho}$, velocity $\tilde{\boldsymbol{u}}$, pressure $\tilde{p}$ and internal energy density $\tilde{e}$.

The ideal gas equation is assumed to be valid:

$$\tilde{p} = \tilde{\varrho}\tilde{R}\tilde{T}. \tag{4}$$

The internal energy density $\tilde{e}_u$ includes the reaction enthalpy $\Delta\tilde{h}_f$. γ is the ratio of specific heats at constant pressure and volume, respectively, $\tilde{c}_p/\tilde{c}_v$:

$$\tilde{e}_u = \frac{\tilde{p_u}/\tilde{\varrho}_u}{\gamma - 1} + \Delta\tilde{h}_f. \tag{5}$$

At $t = t_0$, the gas is at rest and has a uniform initial density $\tilde{\varrho}_i$ and pressure $\tilde{p}_i$. The jump conditions at the interface state that mass, momentum and energy flux are

conserved. Index b denotes quantities at the flame front in the burnt gas, index u in the unburnt gas at the flame front $\tilde{\boldsymbol{x}} = \tilde{\boldsymbol{x}}_f$:

$$\tilde{\varrho}_u \left(\tilde{\boldsymbol{u}}_u - \tilde{\boldsymbol{u}}_f\right) \cdot \boldsymbol{n}_f = \tilde{\varrho}_b \left(\tilde{\boldsymbol{u}}_b - \tilde{\boldsymbol{u}}_f\right) \cdot \boldsymbol{n}_f, \tag{6}$$

$$\left(\tilde{\varrho}_u \tilde{\boldsymbol{u}}_u \left(\tilde{\boldsymbol{u}}_u - \tilde{\boldsymbol{u}}_f\right) + \tilde{p}_u \boldsymbol{I}\right) \cdot \boldsymbol{n}_f = \left(\tilde{\varrho}_b \tilde{\boldsymbol{u}}_b \left(\tilde{\boldsymbol{u}}_b - \tilde{\boldsymbol{u}}_f\right) + \tilde{p}_b \boldsymbol{I}\right) \cdot \boldsymbol{n}_f, \tag{7}$$

$$\left(\tilde{\varrho}_u \left(\tilde{\boldsymbol{u}}_u - \tilde{\boldsymbol{u}}_f\right) \left(\tilde{e}_u + \tilde{u}_u^2/2\right) + \tilde{p}_u \tilde{\boldsymbol{u}}_u\right) \cdot \boldsymbol{n}_f = \left(\tilde{\varrho}_b \left(\tilde{\boldsymbol{u}}_b - \tilde{\boldsymbol{u}}_f\right) \left(\tilde{e}_b + \tilde{u}_b^2/2\right) + \tilde{p}_b \tilde{\boldsymbol{u}}_b\right) \cdot \boldsymbol{n}_f. \tag{8}$$

The flame front velocity $\tilde{\boldsymbol{u}}_f$ is the sum of the velocity of the unburnt gas $\tilde{\boldsymbol{u}}_u$ and the laminar flame speed in normal direction $-\tilde{s}_L \boldsymbol{n}_f$:

$$\tilde{\boldsymbol{u}}_f = \frac{\mathrm{d}\tilde{\boldsymbol{x}}_f}{\mathrm{d}\tilde{t}} = \tilde{\boldsymbol{u}}_u - \tilde{s}_L \boldsymbol{n}_f. \tag{9}$$

where $\tilde{s}_L$ is the laminar flame speed defined as the normal velocity of the flame front with respect to the unburnt gas at the flame front. Following [3], we assume $\tilde{s}_L$ depends on the local curvature $\tilde{\kappa}$ of the flame front and the so–called Markstein length $\tilde{l}_{\mathrm{Ma}}$:

$$\tilde{s}_L = \tilde{s}_{L,0} \left(1 - \tilde{\kappa} \tilde{l}_{\mathrm{Ma}}\right). \tag{10}$$

The Markstein length is assumed to be of the order of the flame thickness[3] and $\tilde{s}_{L,0}$ is constant.

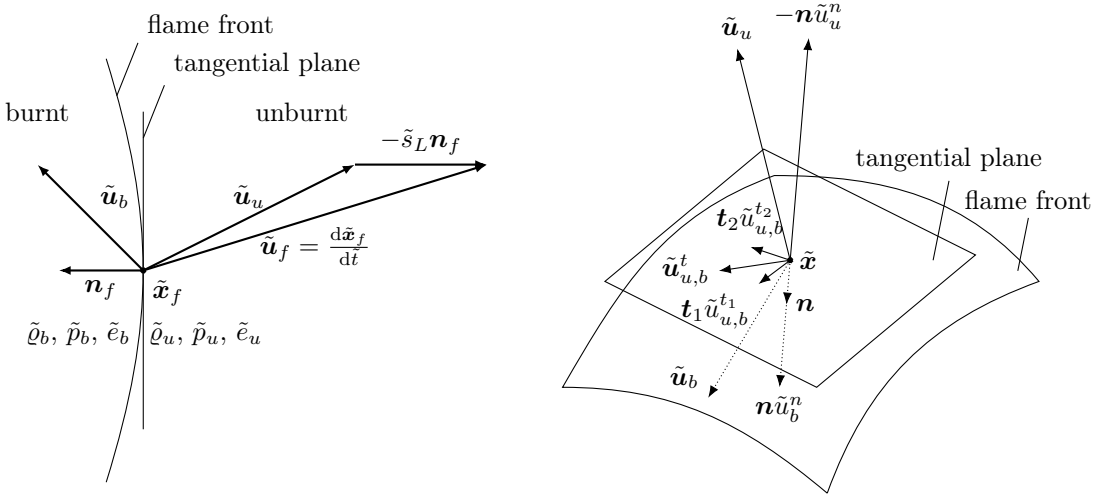

(a) Jump of velocity

(b) Tangential plane and normal direction

Figure 2: Illustration of the jump conditions at the flame front

2.2 Stability of the Flame Front

For the linear stability analysis, a plane flame front is assumed. The dispersion relation for the growth rate $\tilde{\Omega}$ of a disturbance with wavenumber $\tilde{k}$ reads as[3, 7]:

$$(\sigma + 1)\, \tilde{\Omega}^2 + 2 \left(1 + \tilde{k} \tilde{l}_{\mathrm{Ma}}\right) \sigma \tilde{k} \tilde{s}_{L,0} \tilde{\Omega} - \left(\sigma - 1 - 2\tilde{l}_{\mathrm{Ma}} \sigma \tilde{k}\right) \sigma \tilde{k}^2 \tilde{s}_{L,0}^2 = \tilde{0}. \tag{11}$$

where σ is the expansion ratio, defined as $\tilde{\varrho}_u/\tilde{\varrho}_b$. In case of isobaric conditions with uniform temperature in the unburnt gas, it is constant.

To obtain the critical wavenumber $\tilde{k}_c$ we set $\tilde{\Omega} = \tilde{0}$:

$$\tilde{k}_c = \frac{\sigma - 1}{2\tilde{l}_{\mathrm{Ma}}\sigma}. \tag{12}$$

The flame front is stable for perturbations with a wavenumber $\tilde{k} > \tilde{k}_c$, and unstable for $\tilde{k} < \tilde{k}_c$. Thus, the stabilisation mechanism acts as a low-pass filter. Setting $\tilde{l}_{\mathrm{Ma}} = 0$, the laminar flame velocity $\tilde{s}_L$ is constant and the flame front is unconditionally unstable for all perturbation wavelengths (Darrieus–Landau instability).

2.3 Non-dimensional Formulation

We introduce characteristic values to obtain a non-dimensional formulation. Pressure and density are scaled with their initial values. $\tilde{s}_{L,0}$ is the characteristic velocity, and the characteristic length $\tilde{L}$ is problem-dependent, e.g. vessel diameter or channel width. We define $\varepsilon = \tilde{\varrho}_i \tilde{s}_{L,0}^2/\tilde{p}_i = \tilde{s}_{L,0}^2/\tilde{c}_i^2\gamma = \mathrm{Ma}_{\mathrm{ref}}^2/\gamma$, proportional to the square of a reference Mach number $\mathrm{Ma} = \tilde{s}_{L,0}/\tilde{c}_i$, with the speed of sound at initial conditions $\tilde{c}_i$. We get for Equations (1) to (3):

$$\frac{\partial \varrho}{\partial t} + \nabla \cdot (\varrho \boldsymbol{u}) = 0, \tag{13}$$

$$\varepsilon \left(\frac{\partial (\varrho \boldsymbol{u})}{\partial t} + \nabla \cdot (\varrho \boldsymbol{u}\boldsymbol{u}) \right) = -\nabla p, \tag{14}$$

$$\frac{\partial \left(\varrho \left(e + \varepsilon u^2/2\right)\right)}{\partial t} + \nabla \cdot \left(\varrho \boldsymbol{u} \left(e + \varepsilon u^2/2 \right) \right) = -\nabla \cdot (p\boldsymbol{u}), \tag{15}$$

and jump conditions, Equations (6) to (8):

$$\varrho_u \left(1 - \kappa l_{\mathrm{Ma}}\right) = \varrho_b \left(u_f^n - u_b^n \right), \tag{16}$$

$$\varepsilon \left(1 - \kappa l_{\mathrm{Ma}}\right) \varrho_u u_u^n + p_u = p_b + \varepsilon \left(1 - \kappa l_{\mathrm{Ma}}\right) \varrho_b u_b^n, \tag{17}$$

$$\boldsymbol{u}_u^t = \boldsymbol{u}_b^t, \tag{18}$$

$$\frac{p_u/\varrho_u}{\gamma - 1} + \Delta h_f + \varepsilon u_u^2/2 - \frac{p_u u_u^n}{\varrho_u \left(1 - \kappa l_{\mathrm{Ma}}\right)} = \frac{p_b/\varrho_b}{\gamma - 1} + \varepsilon u_b^2/2 - \frac{p_b u_b^n}{\varrho_u \left(1 - \kappa l_{\mathrm{Ma}}\right)}. \tag{19}$$

2.4 Expansion for Small Mach Numbers

We assume that at all times, the maximum speed of the fluid is much smaller than the local speed of sound. Thus, we expand all quantities in terms of small $\varepsilon \ll 1$, e.g.:

$$\varrho = \varrho_0 + \varepsilon \varrho_1 + \dots.$$

For the governing Equations (13) to (15), we obtain in leading order:

$$\frac{1}{\varrho_0} \frac{\mathrm{D}\varrho_0}{\mathrm{D}t} + \nabla \cdot \boldsymbol{u}_0, = 0, \tag{20}$$

$$\nabla p_0 = 0, \tag{21}$$

$$\frac{\gamma}{\gamma - 1} \left(\frac{1}{p_0} \frac{\mathrm{D}p_0}{\mathrm{D}t} - \frac{1}{\varrho_0} \frac{\mathrm{D}\varrho_0}{\mathrm{D}t} \right) = \frac{1}{p_0} \frac{\partial p_0}{\partial t}, \tag{22}$$

and in second order for Equation (14):

$$\frac{1}{\varrho_0}\frac{\mathrm{D}\boldsymbol{u}_0}{\mathrm{D}t} = -\nabla p_1. \tag{23}$$

The leading order jump conditions, Equations (16) to (19), at the flame front read as:

$$\varrho_{u,0}\left(1-\kappa l_{\mathrm{Ma}}\right) = \varrho_{b,0}\left(u^n_{f,0} - u^n_{b,0}\right), \tag{24}$$

$$p_{u,0} = p_{b,0}, \tag{25}$$

$$\boldsymbol{u}^t_{u,0} = \boldsymbol{u}^t_{b,0}, \tag{26}$$

$$\frac{1}{\gamma-1}\left(\frac{\varrho_{u,0}}{\varrho_{b,0}} - \frac{p_{u,0}}{p_{b,0}}\right) = \Delta h_f \frac{\varrho_{u,0}}{p_{b,0}} + \left(1-\kappa l_{\mathrm{Ma}}\right)^{-1}\left(u^n_{b,0} - \frac{p_{u,0}}{p_{b,0}}u^n_{u,0}\right). \tag{27}$$

From Equations (21) and (25), we conclude that the leading order pressure is time-dependent only. We rename $p_0 = \bar{p}$ (thermodynamic pressure) and $p_1 = p'$ (pressure correction. In the following, all other quantities are of leading order.

2.5 Decomposition of the Velocity Field

We decompose the velocity field in an irrotational $\nabla\varphi$ and a divergence-free part $\nabla\times\boldsymbol{\psi}$:

$$\boldsymbol{u} = \nabla\times\boldsymbol{\psi} + \nabla\varphi. \tag{28}$$

The scalar potential φ is governed by:

$$\nabla^2\varphi = \nabla\cdot\boldsymbol{u} = -\frac{1}{\varrho}\frac{\mathrm{D}\varrho}{\mathrm{D}t} = -\frac{1}{\gamma}\frac{1}{\bar{p}}\frac{\mathrm{d}\bar{p}}{\mathrm{d}t}, \tag{29}$$

with one possible particulate solution φ_p:

$$\varphi_p = -\frac{x^2}{2}\frac{1}{\gamma}\frac{1}{\bar{p}}\frac{\mathrm{d}\bar{p}}{\mathrm{d}t}. \tag{30}$$

At the flame front, the homogeneous solution φ_h is continuous, but its normal gradient has a jump. For the vector potential $\boldsymbol{\psi}$, setting $\nabla\cdot\boldsymbol{\psi} = 0$ w.l.o.g., we get:

$$\nabla^2\boldsymbol{\psi} = -\nabla\times\boldsymbol{u} = -\boldsymbol{\omega}. \tag{31}$$

The transport equation for vorticity $\boldsymbol{\omega} = \nabla\times\boldsymbol{u}$ is obtained by taking the curl of Equation (23):

$$\frac{\mathrm{D}\boldsymbol{\omega}}{\mathrm{D}t} = \boldsymbol{\omega}\cdot\nabla\boldsymbol{u} - \boldsymbol{\omega}\nabla\cdot\boldsymbol{u} + \frac{1}{\varrho^2}\nabla\varrho\times\nabla p' = \boldsymbol{\omega}\cdot\nabla\boldsymbol{u} - \boldsymbol{\omega}\nabla\cdot\boldsymbol{u} + \frac{1}{\varrho}\frac{\mathrm{D}\boldsymbol{u}}{\mathrm{D}t}\times\nabla\varrho. \tag{32}$$

The decomposition (28) allows us to solve two easier sub-problems: finding φ and $\boldsymbol{\psi}$. Since we already have a particulate solution to the Poisson Equation (29), we use a boundary element method (panel method[8, 9]) to get the homogeneous solution φ_h. Here, vorticity and vector potential are not considered.

In the unburnt gas, the vorticity always vanishes, $\boldsymbol{\omega} = 0$. However, the vorticity generated by the flame front has an influence on the velocity field in the unburnt fluid. The thermodynamic pressure $\bar{p}$ is a function of time only. Since entropy is conserved (except at the flame front), the density in the unburnt is also time-dependent only.

3 FLAME FRONT TRACKING

The flame front is represented by N marker points $x_{f,i}$, $i = 1, \ldots, N$ (Figure 3a). They move with the flame front according to Equation (9). To fulfill the jump condition for the normal velocity, we prescribe a singular source distribution along the flame front.

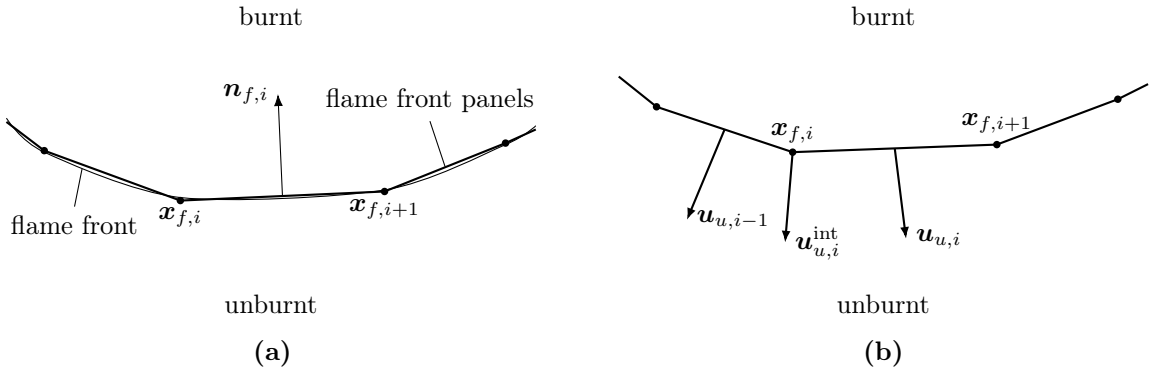

Figure 3: **(a)** Discretisation of the flame front, **(b)** velocity interpolation

3.1 Panel Method

We adapt the panel method described in [8, 9]. The jump of normal velocity Δu_i^n at the flame front is known and equal to the source strength q_f of the flame front:

$$\Big[\nabla\varphi_h(\boldsymbol{x}_f(s)) \cdot \boldsymbol{n}_f(s)\Big] = q_f(s) = \Delta u^n(s) = \frac{\gamma - 1}{\gamma}\left(1 - \kappa(s) l_{\text{Ma}}\right) \Delta h_f \bar{p}^{(1-\gamma)/\gamma}. \tag{33}$$

s is the arc length across the flame front and $[b]$ denotes the jump of a quantity b when crossing the front. When discretised, the jump of normal velocity across a panel i is time-dependent only, $\Delta u_i^n = f(t)$.

3.2 Moving the Flame Front

At every time step, we have to move the flame front points. The discretised kinematic condition for each flame front point $\boldsymbol{x}_{f,i}$ for the time step $(n+1)$ reads as:

$$\boldsymbol{x}_{f,i}^{n+1} = \boldsymbol{x}_{f,i}^n + \Delta t \boldsymbol{u}_{f,i}^n. \tag{34}$$

The velocity $\boldsymbol{u}_u$ induced by the panel method is singular at each panel edge, i.e. marker point. To obtain a smooth approximate velocity field at the marker points, we interpolate the velocity $\boldsymbol{u}_{u,i}^{\text{int}}$ using two adjacent panels i and $i-1$, see Figure 3b:

$$\boldsymbol{u}_{u,i}^{\text{int}} = \frac{l_i \boldsymbol{u}_{u,i-1} + l_{i-1} \boldsymbol{u}_{u,i}}{l_i + l_{i-1}}. \tag{35}$$

where l_i is the length of panel i and $\boldsymbol{u}_{u,i}$ is the velocity of the unburnt gas, evaluated at centre of panel i.

In order to be able to simulate the propagation of a partially unstable flame front, we iteratively reseed the marker points in each time step: Panels that are too short (Figure 4a) or have a too sharp edge (Figure 4b) are cut out, panels that are too long (Figure 4c) are split. Two parameters have to be specified: the average length l_{avg} of one panel, where the actual length of each panel has to lie between $0.5l_{\text{avg}}$ and $2l_{\text{avg}}$ and the minimum angle $\alpha_{\min}$ between two panels.

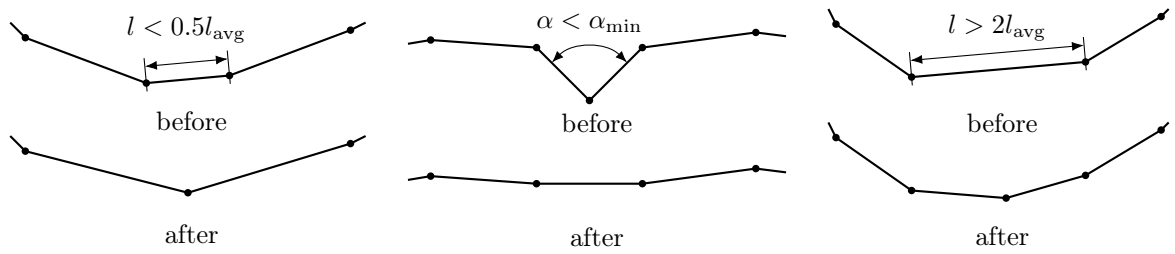

(a) Panel too short **(b)** Panel too sharp **(c)** Panel too long

Figure 4: Stabilisation of the flame front moving algorithm

4 APPLICATIONS

We consider the following two-dimensional problems, Figure 5: (I) a plane flame front in an infinite channel, and (II) combustion in a closed vessel. We represent the two-dimensional space by complex numbers $z = x + iy$, where $\boldsymbol{x} = (x, y)$. The complex velocity is $U = u - iv$, with $\boldsymbol{u} = (u, v)$.

4.1 Infinite Channel

The flame front moves into quiescent, unburnt gas in an infinitely long channel (Figure 5a). At the walls, located at $z_w(y) = \pm 1 + iy$, periodic boundary conditions are applied. The thermodynamic pressure $\bar{p}$ and the expansion ratio σ are constant and the unburnt gas has a uniform temperature distribution.

To fulfill the boundary conditions, we have to apply the method of mirrored panels as outlined in [10, 11]. For the complex velocity U_p at point z induced by a single panel located between two points z_1 and z_2, we get:

$$U_p(z) = \frac{q}{2\pi} \frac{||z_1 - z_2||}{z_1 - z_2} \ln\left(\frac{\sin(\pi/2\,(z - z_2))}{\sin(\pi/2\,(z - z_1))}\right). \tag{36}$$

The total velocity U induced by all panels is the sum of all panel contributions $U_{p,i}$.

4.2 Combustion in a Closed Vessel

A closed vessel is represented by fixed panels (Figure 5b) where the boundary condition of a vanishing normal velocity has to be satisfied. The pressure rises significantly. The integral equation for the pressure change reads as:

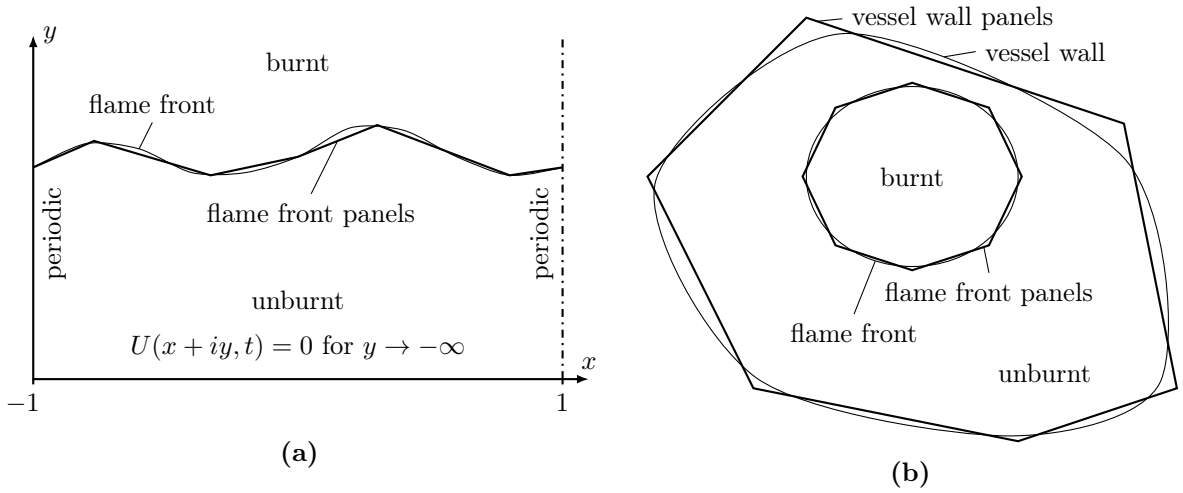

Figure 5: Flame front in **(a)** an infinite channel and **(b)** inside a closed vessel

$$\frac{\mathrm{d}\bar{p}}{\mathrm{d}t} = \frac{\gamma\bar{p}}{V_v}\int_{\text{f.f.}} (u_u^n - u_b^n)\ \mathrm{d}O, \tag{37}$$

where V_v is the volume of the vessel per unit length. Integration is done along the flame front (f.f.). The complex velocity U_p at point z induced by a single panel between points z_1 and z_2 is:

$$U_p(z) = \frac{q}{2\pi}\frac{||z_1 - z_2||}{z_1 - z_2}\ln\left(\frac{z - z_2}{z - z_1}\right). \tag{38}$$

We assume that the vessel wall is adiabatic. Once the flame front touches the wall, the assumption of no heat loss to the surroundings becomes invalid. Thus, we stop the simulation.

5 RESULTS

Although vorticity and vector potential are neglected, the following results illustrate the potential and performance of the presented front tracking method.

5.1 Infinite Channel

Figure 6 shows the stabilisation mechanism due to the Markstein length, with parameters $l_{\text{Ma}} = 0.0416$, $\sigma = 6$, $k_c = 10$, $l_{\text{avg}} = 0.005$, $\Delta t = 10^{-5}$ and $\alpha_{\min} = 120°$.

At $t = 0$, the flame front is sinusoidal with an amplitude $a = 0.01$. If the initial wavenumber k_i is smaller than the critical wavenumber k_c (Figure 6a), the distortion will grow in amplitude, see $t = 0$ to $t = 0.4$. For $t = 0.8$ and $t = 1.0$, low wavenumber instabilities with a larger growth rate than the initial wavenumber develop and become visible.

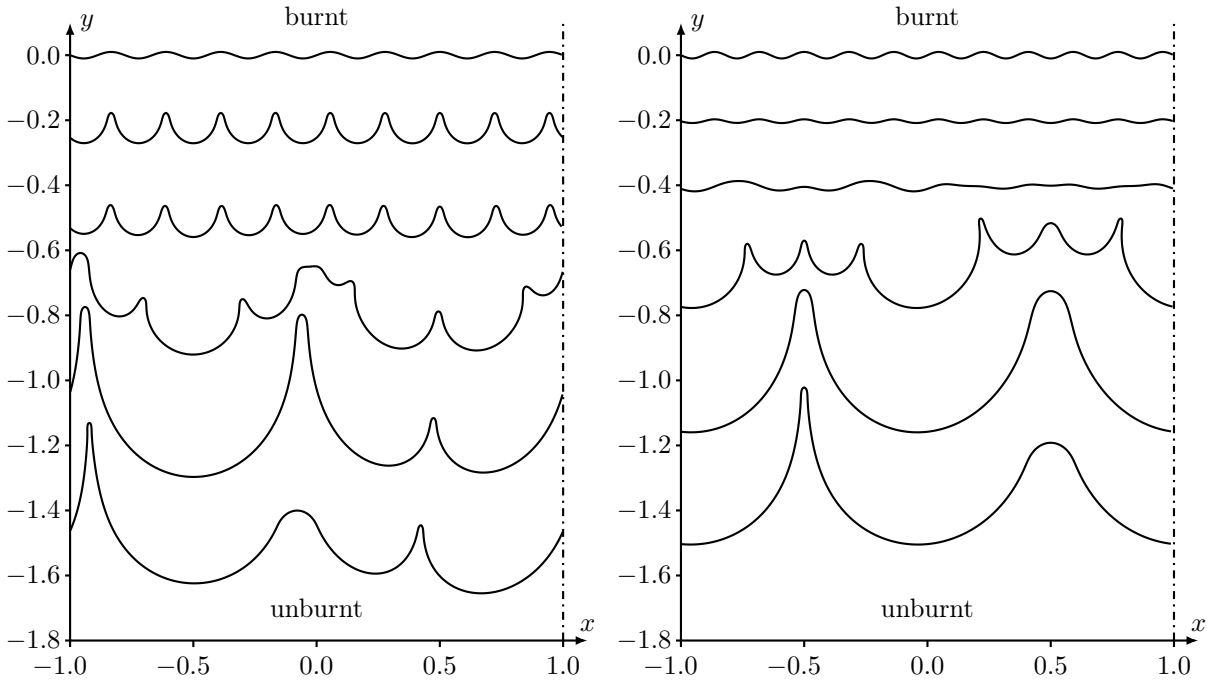

(a) $k_i = k_c - 1$ **(b)** $k_i = k_c + 1$

Figure 6: Planar flame front in a channel, consecutive time intervals with $\Delta t = 0.2$

If the initial wavenumber is higher than the critical wavenumber (Figure 6b), the distortion is damped, $t = 0$ to $t = 0.2$. At $t = 0.4$, low wavenumber instabilities start to grow. At $t = 0.6$, coalescence of instabilities is visible. For $t = 0.8$, unstable modes have developed.

An unperturbed flame front moves with velocity $v = -1$. If it is wrinkled, it is considerably faster. E.g., compare the location of the flame front for $t = 0.2$ and $t = 0.4$ for the wrinkled (left) and almost undisturbed (right) flame front.

5.2 Combustion in a Closed Vessel

Figure 7 shows the flame front inside a rectangular vessel for different times, with parameters $\Delta h_f = 20$, $\gamma = 1.4$, $l_{\text{Ma}} = 0.005$, $l_{\text{avg}} = 0.002$ and $\Delta t = 10^{-6}$. The vessel has a height to width ratio of two to three with rounded corners.

The reaction enthalpy Δh_f is chosen such, that the end pressure, i.e. the pressure after total adiabatic combustion, is about $p_e = 9$, to agree with bomb calorimeter dust explosion experiments[12]. Note, the pressure at the end of the simulation ($t = 0.1577$) shown in Figure 8 is much less than 9, since a large portion of the gas is not burnt yet.

At $t = 0$, the flame front is a circle with radius $r_i = 10^{-2}$ (Figure 7). Note, r_i must be larger than the Markstein length $r_i > l_{\text{Ma}}$, because otherwise the flame would not move.

The flame stays circular until about $t = 0.03$ since the walls of the vessel are still far away. Thus, their influence on the flame front is small. At $t = 0.06$, first deviations from the initial shape are visible and the boundaries begin to have an impact on the interface.

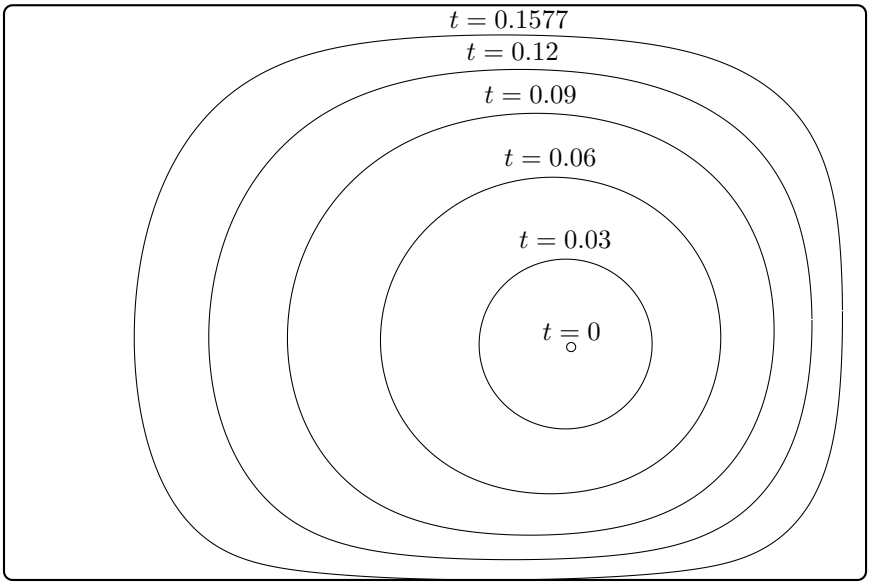

Figure 7: Flame front position for confined combustion in a rectangular vessel

Once the flame touches the wall, $t = 0.1577$, the simulation stops.

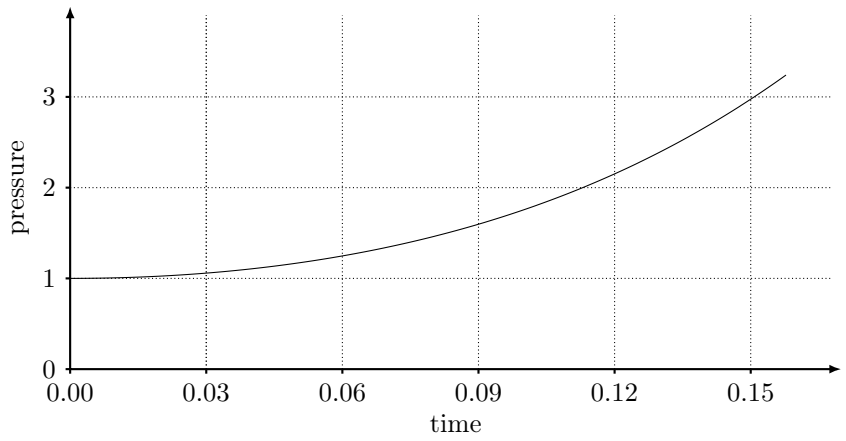

Figure 8: Pressure rise for confined combustion in a rectangular vessel

Figure 8 shows the evolution of the pressure in time. Since the pressure change depends on the current pressure, $\bar{p}$ increases exponentially, cf. Equation (37).

6 DISCUSSION

A new method to track the flame front of slow combustion has been developed and successfully implemented. The implementation shows good performance and uses modern parallelisation techniques to enable fast simulations.

The evolution of an initially slightly perturbed flame front in an infinite channel is in good qualitative agreement with CFD results using a level-set method, compare Figure 6a, time $t = 0.2$ with Figure 10 from [7]. The stability limit from our simulations match those

from [3, 7]. We obtain a similar shape of a single wrinkle. However, the method proposed here is simpler and faster.

For combustion in a close vessel, the Markstein length was large enough to damp all instabilities. Additionally, the pressure rise of combustion in a vessel is in good agreement with experiments[12, 13].

Numerical dissipation of the front tracking method presented here is considerably lower than that of other methods. Our method resolves the flame front as discontinuity. In level-set and front tracking methods, the interface is approximated by finite-sized cells which do not necessarily coincide with the flame front shape. Thus, it is smeared over multiple mesh cells.

In addition to the model instability, a numerical instability arises due to the low numerical dissipation of the proposed front tracking method. If not controlled, this leads to unphysical behaviour of the flame front. Self-intersections of the flame front can occur. Our stabilisation algorithm successfully suppresses the numerical instabilities of the moving algorithm, with the right choice of parameters.

The minimal angle between two neighbouring panels $\alpha_{\min}$ and the average panel length l_{avg} need to be carefully adjusted. Too small values of $\alpha_{\min}$ would allow overturning of neighbouring flame front panels. For sufficiently low average panel lengths, the angle of a single wrinkle is smaller than $\alpha_{\min}$. Here, we chose $\alpha_{\min}$ such, that the front moving algorithm remains stable. l_{avg} was chosen that all unstable wavelengths can be captured with good accuracy and no aliasing.

Currently, the velocity induced by vorticity generation is neglected. The implementation is current work in progress. For the planar flame front, vorticity can only be generated at the flame front. There is no density gradient in the burnt gas and the right-hand side of the vorticity transport Equation (32) is identical to zero. In confined combustion, there is a non-vanishing divergence of the velocity field and a significant density gradient in the burnt gas[14]. Thus, the vorticity of a material element increases even after passing the flame front.

For simple flame models, the front tracking method described here leads to simulation results comparable to literature in short simulation times. We plan to extend our implementation to account for rotational symmetric geometries and different boundary conditions at the vessel wall.

REFERENCES

[1] Darrieus, G., Propagation d'un front de flamme. Presented at *Le Congrés de Mécanique Appliquée* (1945), Paris.

[2] Landau, L.D., On the theory of slow combustion, *Acta Physicochim. URSS* (1944), **19**:77–85.

[3] Markstein, G.H., *Nonsteady flame propagation*. Pergamon Press, 1964.

[4] Shivashinsky, G.I., On a distorted flame front as a hydrodynamic discontinuity, *Acta Astronaut.* (1976), **3**(11-12):889–918.

[5] Matalon, M. and Matkowsky, B.J., Flames as gasdynamic discontinuities, *J. of Fluid Mech.* (1982), **124**:239–259.

[6] Class, G.A., Matkowsky, B.J. and Klimenko, A.Y., A unified model of flames as gasdynamic discontinuities, *J. of Fluid Mech.* (2003), **491**:11–49.

[7] Rastigejev, Y. and Matalon, M., Nonlinear evolution of hydrodynamically unstable premixed flames, *J. of Fluid Mech.* (2006), **554**:371–392.

[8] Katz, J. and Plotkin, A., *Low-Speed Aerodynamics*, Cambridge University Press, 2nd Edition, 2001.

[9] Cebeci, T., *An Engineering Approach to the Calculation of Aerodynamic Flows*, Springer Verlag, 1999.

[10] Schneider, W., *Mathematische Methoden der Strömungsmechanik*. Vieweg, 1978.

[11] Greengard, L., Potential flow in channels, *SIAM J. Sci. and Stat. Comput.* (1990), **11**(4):603–620.

[12] Ogle, R.A., *Dust Explosion Dynamics*, Butterworth–Heinemann, 2017.

[13] Tang, C., Zhang, S., Si, Z., Huang, Z., Zhang, K. and Jin, Z., High methane natural gas/air explosion characteristics in confined vessel, *J. Hazard. Mater.* (2014), **278**:520–528.

[14] Lewis, B. and von Elbe, G., *Combustion, Flames and Explosion of Gases*, Academic Press, 2nd Edition, 1961.